

Finding the Hidden Valence Band of N=7 Armchair Graphene Nanoribbons with Angle-Resolved Photoemission Spectroscopy

Boris V. Senkovskiy,^{1,2,*} Dmitry Yu. Usachov,² Alexander V. Fedorov,^{3,2}
Danny Haberer,⁴ Niels Ehlen,¹ Felix R. Fischer,^{4,5,6} and Alexander Grüneis^{1,†}

¹*II. Physikalisches Institut, Universität zu Köln, Zùlpicher Straße 77, 50937 Köln, Germany*

²*St. Petersburg State University, 7/9 Universitetskaya nab., St. Petersburg, 199034, Russia*

³*IFW-Dresden, Dresden, Helmholtzstraße 20, 01069, Germany*

⁴*Department of Chemistry, University of California at Berkeley,
Tan Hall 680, Berkeley, CA 94720, United States*

⁵*Materials Science Division, Lawrence Berkeley National Laboratory, Berkeley, California 94720, United States*

⁶*Kavli Energy Nanosciences Institute at the University of California Berkeley and
Lawrence Berkeley National Laboratory, Berkeley, California 94720, United States*

To understand the optical and transport properties of graphene nanoribbons, an unambiguous determination of their electronic band structure is needed. In this work we demonstrate that the photoemission intensity of each valence sub-band, formed due to the quantum confinement in quasi-one-dimensional (1D) graphene nanoribbons, is a peaked function of the two-dimensional (2D) momentum. We resolve the long-standing discrepancy regarding the valence band effective mass (m_{VB}^*) of armchair graphene nanoribbons with a width of N=7 carbon atoms (7-AGNRs). In particular, angle-resolved photoemission spectroscopy (ARPES) and scanning tunneling spectroscopy report $m_{VB}^* \approx 0.2$ and ≈ 0.4 of the free electron mass (m_e), respectively. ARPES mapping in the full 2D momentum space identifies the experimental conditions for obtaining a large intensity for each of the three highest valence 1D sub-bands. Our detail map reveals that previous ARPES experiments have incorrectly assigned the second sub-band as the frontier one. The correct frontier valence sub-band for 7-AGNRs is only visible in a narrow range of emission angles. For this band we obtain an ARPES derived effective mass of $0.4 m_e$, a charge carrier velocity in the linear part of the band of 0.63×10^6 m/s and an energy separation of only ≈ 60 meV to the second sub-band. Our results are of importance not only for the growing research field of graphene nanoribbons but also for the community, which studies quantum confined systems.

I. INTRODUCTION

When a two-dimensional (2D) material is scaled down to a quasi-one-dimensional (1D) ribbon, its electronic structure changes dramatically due to the quantum confinement of the electron wave functions. Graphene nanoribbons (GNRs) have a band gap and a tunable electronic structure, and therefore they are a promising material for opto-electronic applications. After the discovery of bottom-up synthesis which allows atomically precise fabrication,¹ there is a boom in design and study of GNRs.^{2–21} The first reported¹ and the most studied system is the semiconducting armchair graphene nanoribbons of N=7 carbon atoms width (7-AGNRs). The conductance of individual 7-AGNRs was measured²² and the field-effect transistor was fabricated.²³ A wide tunability of the electronic and optical properties of 7-AGNRs was demonstrated. Particularly, it was shown that the decoupling of 7-AGNRs from the metal substrate affects the band gap.^{15,24} The 7-AGNRs can be efficiently functionalized by edge groups,²⁰ by periodically incorporated boron atoms along the ribbon backbone^{6,7} and transformed to a metal by Li-doping.²⁵ Excitonic effect³ and defect-induced photoluminescence¹⁶ were observed. Atomically precise heterojunctions with 7-AGNRs have been also studied.^{5,19,26,27} Thus, electronic band structure of this material seems to be well understood.

However, this is not the case. The electronic band

structure of 7-AGNRs consists of 1D sub-bands with parabolic energy-momentum relation $E(\mathbf{k})$ at the valence band maximum characterized by the effective mass $m_{VB}^* = \hbar^2(\partial^2 E/\partial \mathbf{k}^2)^{-1}$. The effective mass is an important parameter characterizing a semiconductor and there is a large discrepancy in the value of m_{VB}^* as determined by different experimental techniques. Linden et al.²⁸ demonstrated that the synthesis on a vicinal surface Au(788) provides long-range alignment of 7-AGNRs, since the surface-assisted assembling of the ribbons from molecular precursors is confined within narrow (≈ 3.8 nm) Au(111) terraces. This alignment allowed to perform first experimental investigation of the energy band dispersion of 7-AGNRs by means of angle-resolved photoemission spectroscopy (ARPES). Two valence sub-bands with ≈ 0.3 eV energy separation and the same effective mass approximately equal to the free electron mass m_e were extracted from the spectra.²⁸ The work of Ruffieux et al.²⁹ demonstrated ARPES measurements of a better quality and revealed three frontier sub-bands with $m_{VB}^* \approx 0.2 m_e$. Similar energy band dispersion was later reported by other authors.^{25,30,31} On another hand, Fourier-transformed scanning tunneling spectroscopy (FT-STs), where the $E(\mathbf{k})$ is determined from the interference pattern of the electronic waves reflected from the ribbon edges, found $m_{VB}^* \approx 0.4 m_e$.³² The recent ARPES results of various groups agree to one another,^{25,29–31} making erroneous measurements an

unlikely explanation. The discrepancy between ARPES and STS is quite surprising, since both methods actually should lead to identical results. For example, for 9-AGNRs it was found that ARPES and STS reveal the same value of the effective mass of $m_{VB}^* \approx 0.1 m_e$.^{31,33} It is important to understand this issue, since ARPES is a widely used technique to examine the 1D band structure of GNRs^{25,28-31,33} and self-assembled polymeric nanowires.³⁴⁻³⁶

The present manuscript resolves this discrepancy by revealing strong anisotropy in the photoemission intensity of aligned 7-AGNRs, which makes it impossible to identify all sub-bands in a single ARPES scattering geometry. We demonstrate experimentally, that the photoemission matrix element in 1D nanoribbons is a peaked function of the two-dimensional (2D) electron momentum in the ribbon plane. This knowledge allows us to visualize the highest three valence sub-bands and determine important parameters for the transport and optical properties, such as effective masses, energy band offsets and the charge carrier velocities. In previous ARPES data the second-highest sub-band of 7-AGNRs was mistakenly considered as the highest one.^{25,29-31} Our results highlight that proper application of the ARPES technique for probing the electronic structure of confined systems requires careful consideration of photoemission matrix elements.

II. RESULTS AND DISCUSSION

The 1D electronic structure of graphene nanoribbons in tight-binding (TB) model is given by cutting the 2D graphene band structure along confinement lines in momentum space (zone-folding approximation). We introduce the parallel (k_{\parallel}) and the transverse component (k_{\perp}) in the 2D momentum space. Each cutting line at fixed k_{\perp} determines the allowed momentum for a N-AGNR and leads to 1D bands below and above the Fermi level with band indices $n = 1, \dots, N$, where $N = 7$ is the number of atoms along the width of nanoribbon, as it is shown for 7-AGNRs in Fig. 1. ARPES directly reveal energy band dispersion along the defined direction in k -space. If the ribbons are oriented along the vertical slit of analyzer, the scans will be acquired in some range of k_{\parallel} (Fig. 1). Using the tilt angle one can move the center of the scan along k_{\parallel} , for example, from the Γ (tilt = 0°) to the M point of graphene's BZ, which corresponds to moving from the center of the first to the center of the second 1D BZ of 7-AGNR. By rotating the sample around the polar axis we can change k_{\perp} .

Due to quantum confinement the amplitude of the wave function in the direction perpendicular to nanoribbon axis is changing as $\sin(q_{\perp}^n a/2)$, where $q_{\perp}^n = \frac{2\pi n}{a(N+1)}$ is the quantized value of k_{\perp} and a is the lattice constant of graphene.³⁷⁻³⁹ If the final state in the photoemission process is assumed to be a plane wave, then the photoemission matrix element for the π states of GNR in the dipole approximation can be expressed as³¹

$$M(\mathbf{k}) \propto \sum_j e^{-ik_{\perp} R_{j\perp}} C_j(k_{\parallel}), \quad (1)$$

where $R_{j\perp}$ are the transverse components of atomic coordinates and $C_j(k_{\parallel})$ are the Bloch wave function amplitudes for the π states. Here, we neglected the factors related to the photon polarization direction and to the photoionization cross section of $2p_z$ atomic orbitals. The coefficients in Eq. 1 in TB model can be written as³⁷

$$C_A \propto \sin \frac{mq_{\perp}^n a}{2}, \quad C_B = \pm C_A \left(\frac{|f_n(k_{\parallel})|}{f_n(k_{\parallel})} \right), \quad (2)$$

where C_A and C_B refers to the graphene sub-lattices A and B, \pm stands for the conduction and valence bands, correspondingly, m is the number of atomic row along the ribbon width, $f_n(k_{\parallel}) = -\gamma(2e^{ik_{\parallel}a/2\sqrt{3}} \cos(aq_{\perp}^n/2) + e^{-ik_{\parallel}a/\sqrt{3}})$ and $\gamma \approx 2.8$ eV is the absolute value of the hopping integral. Within TB approximation the sum in Eq. 1 is a Fourier transform of the sine-like wave confined along the ribbon width. Therefore, the intensity $I(\mathbf{k}) \propto |M(\mathbf{k})|^2$ must have strong maxima when the projection of the photoelectron wave vector onto the direction perpendicular to the ribbon axis and parallel to the surface matches the values of $\pm q_{\perp}^n$. It is similar to the momentum quantization in the ARPES spectra of ordered molecular systems.⁴⁰⁻⁴² The photoemission intensity modulation with a change in the emission angle is also well known for the 1D quantum well electronic states confined within nm-scale terraces of stepped noble metal surfaces.^{43,44} Substituting the coefficients Eq. 2 in the equation Eq. 1 and taking into account the life time broadening, we can qualitatively describe the photoemission intensity of the valence sub-band n by the following analytical expression

$$I_n(E, k_{\parallel}, k_{\perp}) \propto \frac{\beta}{(E + |f_n(k_{\parallel})|)^2 + \beta^2} \left| \sum_{m=1}^N e^{-imk_{\perp}a/2} \sin \frac{mq_{\perp}^n a}{2} \left(1 - \frac{|f_n(k_{\parallel})|}{f_n(k_{\parallel})} \right) \right|^2, \quad (3)$$

where β is the lifetime broadening of bands. The last factor in the sum is related to a phase shift between the wave functions of electrons emitted from the two different sub-lattices and accounts for anisotropic intensity in the ARPES studies of graphene.⁴⁵⁻⁵¹

To probe the intensity variation of 1D sub-bands we set up the ARPES geometry as depicted in Fig. 1. The Au(788) crystal with aligned ribbons is oriented to measure the ARPES spectra along the GNR axis. Figure 2 shows the ARPES scans along k_{\parallel} at different k_{\perp} , as it is illustrated in the inset of each panel. We start with a scan at $k_{\perp} = 0 \text{ \AA}^{-1}$ (Fig. 2 a), that is along the ΓM direction of the graphene's BZ, where the parabolic sub-band VB₃ is observed with the maximal intensity. As we

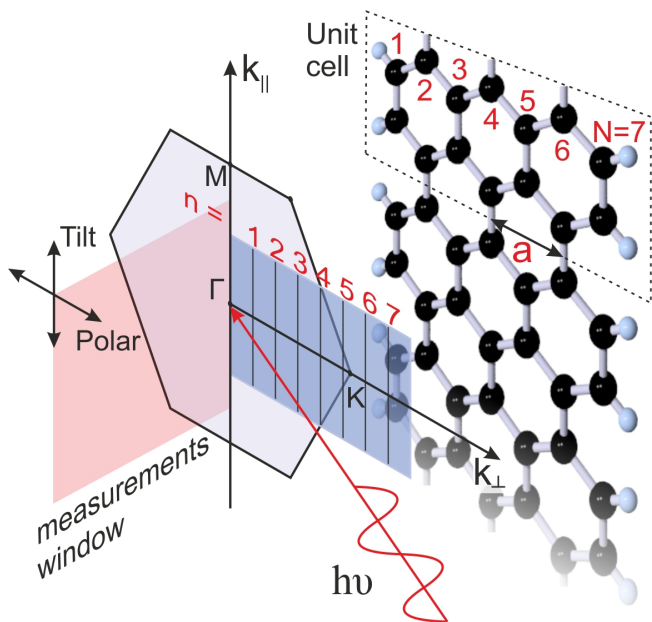


Figure 1. Sketch of the ARPES experiment and the structure of hydrogen-terminated 7-AGNR with $a = 2.46$ Å. The cutting lines of 7-AGNR inside the unfolded 1D BZ with band indices $n = 1, \dots, 7$ and the 2D BZ of graphene are shown. The measurements plane is aligned vertically along the ribbons. The center of the scan is adjusted along k_{\parallel} by the tilt angle, while k_{\perp} is changed by the polar angle. The horizontally polarized light with a photon energy of 45 eV is utilized.

will show later that is the third 1D sub-band of 7-AGNRs (here we count sub-bands from the Fermi level onwards). The next sub-band VB_2 is hard to see in this geometry and its intensity rises when we increase k_{\perp} (Fig. 2 b). At higher values of k_{\perp} (Fig. 2 c), the third sub-band loses its intensity and the highest sub-band VB_1 appears, which determines the VB maximum. This sub-band acquires the intensity in the first 1D BZ when we move the scans along the transverse momentum component further, as it is displayed in the panel (d) of Fig. 2. Thus, the photoemission intensity of sub-bands is strongly dependent on k_{\perp} . This effect is similar to the intensity oscillations of π -bands of multilayer graphene, where the out-of-plane momentum is quantized.⁵²

Figure 3 (a) shows the distribution of photoemission intensity in k -space obtained from the TB model using the analytical Eq. 3 at the constant binding energy (1.89 eV). The energy of the valence band maximum in TB calculations is aligned to the experimental energy of VB_1 apex. The orientation of k_{\perp} axis is horizontal in accordance with the experimental geometry (Fig. 1). The labeled cutting lines indices $n = 5, 6$ and 7 of 7-AGNRs (see Fig.1) correspond to the three highest valence sub-bands VB_1, VB_2 and VB_3 , respectively. Similar picture of the ARPES intensity is obtained with Eq. 1 based on the DFT wave functions of freestanding 7-AGNR (Fig. 3 b). Both theoretical approaches indicate that for each 1D sub-band of 7-AGNR there is a narrow range of k_{\perp}

where we expect a strong photoemission intensity. Figure 3 (c) shows the experimental constant energy slice of the ARPES map of 7-AGNRs on Au(788), which demonstrates an excellent agreement of the experiment and the theory. In supplementary information we present the theoretical and experimental constant energy cuts of the ARPES map at energies close to the valence band maximum of 7-AGNRs. The peaked distribution of the photoemission intensity for GNRs is different from the case of 2D graphene, where the intensity of π -band changes smoothly in ARPES map around the K point.⁴⁶⁻⁵⁰

Note that the TB approach is also applicable to the FT-STs measurements and predicts that it is difficult to resolve those sub-bands for which the wave function changes its sign once per unit cell along the ribbon axis.³³ This could be the reason why for 7-AGNRs the second valence sub-band was not visible in FT-STs data.³²

Now we compare the experimental and the calculated band dispersion. Fig. 4 (a) shows the scan, where the two sub-bands VB_2 and VB_3 can be simultaneously observed. The black dots indicate the DFT-derived bands with the valence band maximum adjusted to the experimental energy of VB_1 . Here we can see qualitative agreement in the dispersion of VB_2 and VB_3 for 7-AGNRs on Au with the calculations for freestanding system. However quantitatively there is a difference, particularly, the maximum of VB_2 in experiment is obviously closer to the Fermi level (see Table 1).

Since the first valence sub-band VB_1 is resolved in the first 1D BZ, it can be measured with a tilt = 0° , as shown in Fig. 4 (b), and its effective mass as well as the energy position of the maximum can be reliably extracted. The white curve shows the fitting points obtained from the energy distribution curves (EDCs). The highest sub-band can be fitted by a parabola only in the vicinity (≈ 60 meV) of the apex, where we obtain an effective mass of $m_{VB_1}^* = 0.40 \pm 0.04 m_e$ and an energy of $E_{VB_1} = 0.87 \pm 0.03$ eV for the VB maximum. It can be seen in Table 1 that these values are in good agreement with the reported FT-STs data for 7-AGNRs/Au(111).³² We also found that already at ≈ 250 meV below the maximum, the dispersion of the first sub-band becomes linear. From the linear slope we extract the charge carrier velocity $v = \hbar^{-1} \partial E / \partial k_{\parallel} = 0.63 \pm 0.05 \times 10^6$ m/s, which is smaller than the experimental value for freestanding (1.05×10^6 m/s)⁵⁴ and Au(111) supported (1.2×10^6 m/s)⁵⁵ graphene, as well as the value determined for the second sub-band of 7-AGNRs in ARPES data (0.82×10^6 m/s).²⁹

The small separation between the first and the second sub-band of ≈ 60 meV suggests that in the case of hole doping both of them may play a role in the transport properties of the material, while the third sub-band is too low to contribute. This is in a qualitative agreement with the DFT data, revealing small energy separation between the two highest valence sub-bands. It should be noted that the values of the extracted effective masses for the first and second valence sub-bands are very close to

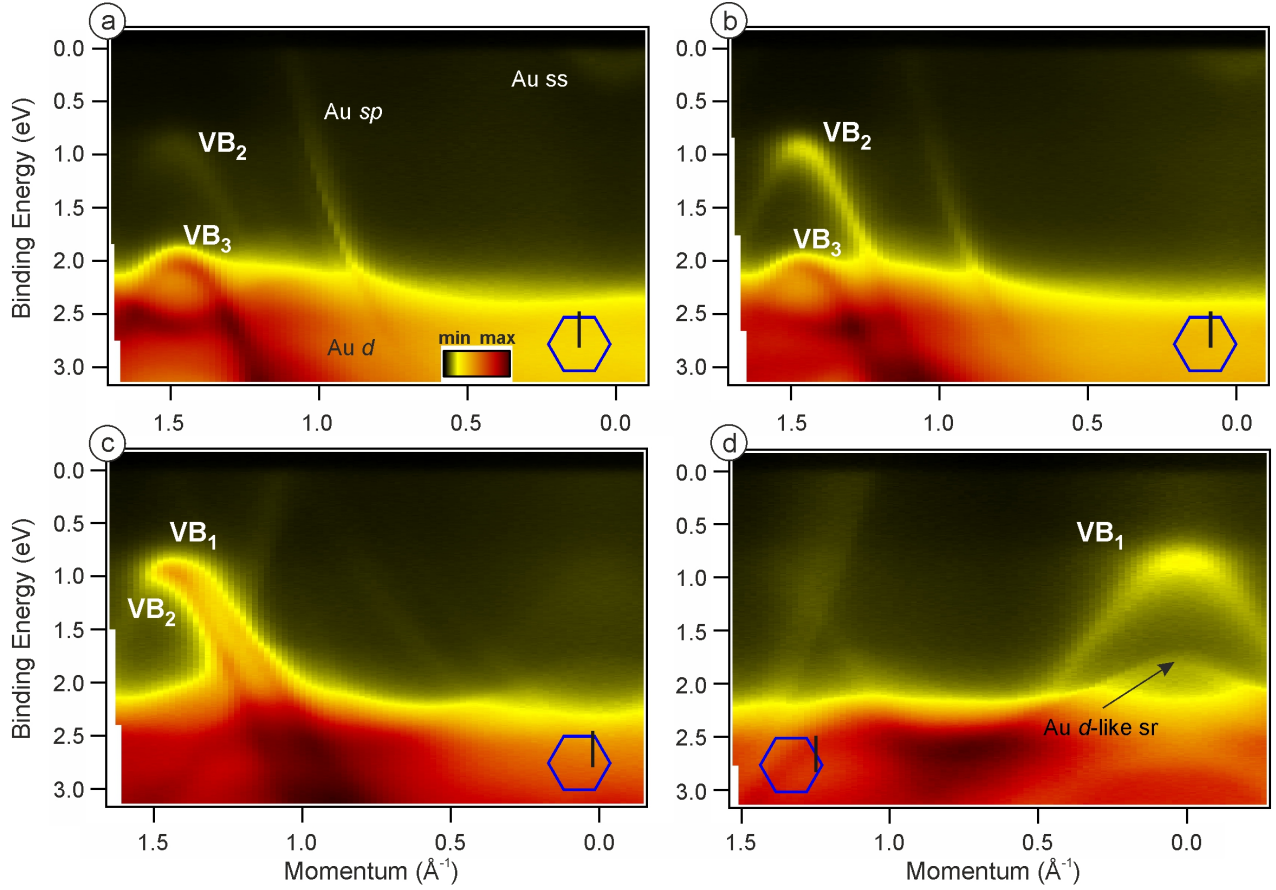


Figure 2. ARPES scans of 7-AGNRs/Au(788) along k_{\parallel} at fixed $k_{\perp} = 0 \text{ \AA}^{-1}$ (a), 0.3 \AA^{-1} (b), 0.75 \AA^{-1} (c), 1.35 \AA^{-1} (d). The insets indicate the scan paths (black vertical line) relative to the BZ of graphene. The sequence of the 1D sub-bands of 7-AGNR relative to the Fermi level is VB_1 , VB_2 and VB_3 . The sub-bands with lower energies are not visible because of overlap with the substrate states. The Au sp - and d -states, as well as the surface state (ss) and surface resonance (sr) are marked.⁵³

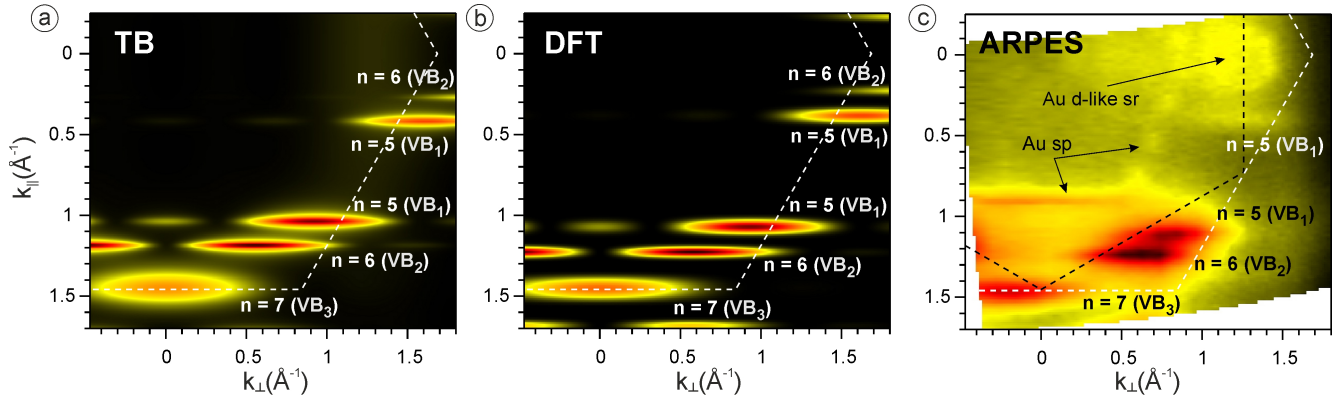


Figure 3. ARPES intensity at binding energy of 1.89 eV from (a) TB and (b) DFT calculations, (c) experiment. The energy scale in DFT and TB calculations was rigidly shifted to align the experimental and calculated valence band maxima. The black and white dashed lines depict the BZs of Au(111) and graphene, correspondingly. The cutting line indices $n = 5, 6, 7$ derived from TB approximation and corresponding sub-bands VB_1, VB_2 and VB_3 are shown. The calculated bands were broadened with $\beta = 0.1 \text{ eV}$ to compare with the experiment.

the values for the corresponding conduction sub-bands obtained from FT-STES measurements, $m_{CB1}^* = 0.40 \pm 0.18 m_e$ and $m_{CB2}^* = 0.20 \pm 0.03 m_e$.³² Taking into account that theory predicts approximately symmetric band structure for the valence and conduction bands, it also testifies to the validity of our results.

Finally, we would like to address the possible reasons why the frontier sub-band VB_1 was not captured in previous ARPES experiments. As we demonstrated, the full k-space ARPES map of a high resolution is needed to assign the experimentally observed sub-bands of GNRs to the theoretical ones. Here we used hemispherical analyzer with the vertical slit (parallel to the manipulator) to measure scan along the direction of 7-AGNRs alignment and the polar angle to tune k_{\perp} . Similar approach can be realized by the analyzer with horizontal slit (most commonly used in ARPES setups) and GNRs aligned along the slit. Then the tilt or azimuthal angle for mapping in 2D k-space can be used. As it is shown in Fig. 3 and Fig. 2 (a), if one measure strictly along the ribbons axis ($k_{\perp} = 0$) or slightly off (if there is a small deviation in tilt or azimuthal angle for horizontal orientation) the VB_3 and VB_2 should be seen. Indeed, such a picture was observed in previous data.^{25,29,30} It is intuitive to measure along the ribbon axis, but in this case VB_1 is not visible. When VB_1 is well observed in the scan, the third sub-band VB_3 loses its intensity (Fig. 3 and Fig. 2 c). Note, that to measure VB_1 in first 1D BZ, as shown in Fig. 2 (d), in horizontal orientation one have to apply large tilt angle ($\approx 25^\circ$ for photon energy of 45 eV), which demands specially designed sample manipulator in ARPES setup. In additional to the experimental configuration, the important issue is the sample itself. Previously, an additional feature was observed in ARPES and taken for the second sub-band VB_2 .^{25,29,30} However, this feature is energetically closer to the lowest measured band (VB_3) than to the topmost one, while theory predicts relatively small (≈ 0.2 eV) energy separation between VB_2 and VB_1 (see Table 1) and large separation between VB_2 and VB_3 (≈ 1 eV).^{1,28} Moreover, as we mentioned above, theory and FT-STES data are in good agreement with respect to the conduction sub-bands.³² Thus, it is unlikely that the observed feature belongs to 7-AGNRs. We suppose that this additional band may be attributed to the electronic states of conjugated 7-AGNRs, particularly N=14 and N=21 AGNRs (two and three fused 7-AGNRs, correspondingly). Indeed, when 7-AGNRs are placed close to each other on Au(111) substrate, their wide derivatives at evaluated temperatures²⁶ or during the long annealing time¹⁹ can be produced. Note, that prior to the ARPES measurements the samples should be degassed by annealing after the transfer from ambient conditions. To avoid possible fusion of 7-AGNRs and appearance of additional bands in our spectra, we synthesized our samples *in situ* and carefully performed the last step of the synthesis (cyclodehydrogenation) of 7-AGNRs on Au(788) at $380 \pm 10^\circ\text{C}$ for 15 minutes.

III. CONCLUSIONS

In summary, we have measured ARPES maps of 7-AGNRs and revealed a strong dependence of photoemission matrix elements for 1D valence sub-bands with respect to the experimental geometry. The experimental results together with DFT and tight binding calculations demonstrate that each of the three topmost sub-bands can be selectively visualized by measuring along the ribbon axis with properly chosen transverse momentum. It is shown that the frontier valence sub-band is very close (≈ 60 meV) to the second one and can be probed in the first BZ of 7-AGNRs, that allows reliable extraction of the effective mass value for the charge carriers in 7-AGNRs of $m_{VB}^* \approx 0.4 m_e$, thus eliminating the old discrepancy between ARPES and STS data. The experimental approach used should be also applied for ARPES studies of other types of atomically precise GNRs and nanoribbons of other 2D materials to unambiguously reveal their band structure, which is a key to electronic and optical properties.

IV. EXPERIMENTAL DETAILS

The measurements have been performed at synchrotron HZB BESSY-II at UE112-PGM2 beamline using the 1²-ARPES endstation, which is equipped with the 6 axes manipulator and the hemispherical Scienta R8000 analyzer with a vertical slit parallel to the manipulator. All spectra are taken at room temperature with p (horizontally) polarized light using the photon energy of 45 eV. During the experiment the base pressure was below 2×10^{-10} mbar. The aligned 7-AGNRs on Au(788) were synthesized *in situ* using the bottom-up approach.²⁸

V. THEORETICAL DETAILS

The photoemission intensity was calculated using the dipole approximation for matrix element and the plane wave as a final state.³¹ Density-functional-theory (DFT) calculations were carried out using the FPLO-14.00-48 code (improved version of the original FPLO code by Koepernik and Eschrig⁵⁶) utilizing the generalized gradient approximation (GGA) to the exchange-correlation potential. The ribbons were assumed freestanding and hydrogen-terminated. A k-point grid of $12 \times 1 \times 1$ was used to sample the BZ. Atomic positions were relaxed until the forces on each atom were less than 10^{-2} eV/Å.

ACKNOWLEDGMENTS

B.V.S., A.V.F. and A.G. acknowledge the ERC grant no. 648589 'SUPER-2D', funding from DFG projects CRC 1238 (project A1) and GR 3708/2-1. D.Yu.U., B.V.S. and A.V.F. acknowledge Saint Petersburg State

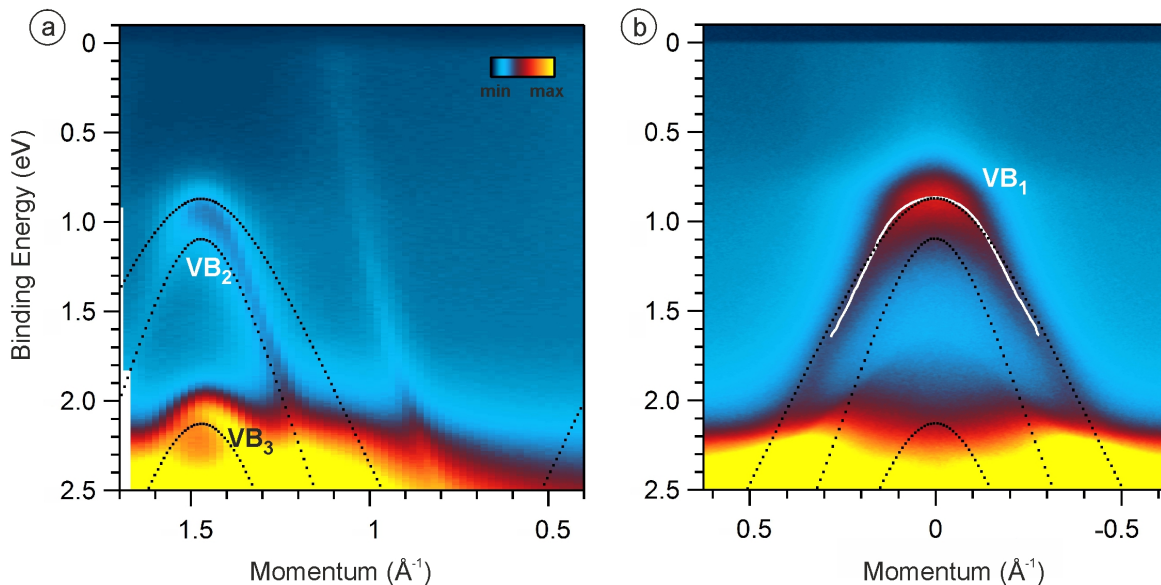


Figure 4. (a) The valence sub-bands VB_3 and VB_2 measured in the second BZ of 7-AGNRs along k_{\parallel} with $k_{\perp} = 0.2 \text{ \AA}^{-1}$. The black dashed lines show the DFT calculated bands. (b) The frontier valence sub-band VB_1 measured in the first BZ of 7-AGNRs along k_{\parallel} with $k_{\perp} = 1.5 \text{ \AA}^{-1}$. The white curve indicates the fitting of the EDCs.

Table I. Energies of the band maxima regarding to the Fermi level and the effective masses for the first (VB_1) and the second (VB_2) valence sub-bands of 7-AGNRs on Au(111) or Au(788).

	ARPES ^a	DFT ^a	FT-STES ³²	previous ARPES ^b
E_{VB1} [eV]	0.87 ± 0.03	0.87	0.84 ± 0.03	—
m_{VB1}^* [m_e]	0.40 ± 0.04	0.33	0.41 ± 0.08	—
E_{VB2} [eV]	0.93 ± 0.03	1.09	—	$0.7^{29}, 0.9^{30}, 0.88^{25}, 0.95^{31}$
m_{VB2}^* [m_e]	0.20 ± 0.04	0.15	—	$0.21^{29}, 0.23^{25}, 0.22^{31}$

^a This work. The binding energy of VB_1 in DFT calculations was chosen equal to the experimental value (0.87 eV).

^b We assume that in previous works the second sub-band was erroneously assigned as the first one.

University for research Grant No. 11.65.42.2017. Research supported by the U.S. Department of Energy (DOE), Office of Science, Basic Energy Sciences (BES), under Award no. DE-SC0010409 (design, synthesis and characterization of molecular building blocks) and the Center for Energy Efficient Electronics Science NSF Award 0939514 (SPM imaging and spectroscopy). The

research leading to these results has received funding from the European Community's Seventh Framework Programme (FP7/2007-2013) under grant agreement n.312284 (CALIPSO). The authors thank HZB BESSY II for the beamtime allocation. This work has been supported by the University of Cologne through the Institutional Strategy of the University of Cologne within the German Excellence Initiative.

* senkovskiy@ph2.uni-koeln.de

† grueneis@ph2.uni-koeln.de

¹ Jinming Cai, Pascal Ruffieux, Rached Jaafar, Marco Bieri, Thomas Braun, Stephan Blankenburg, Matthias Muoth, Ari P. Seitsonen, Moussa Saleh, Xinliang Feng, Klaus Müllen, and Roman Fasel. Atomically precise bottom-up fabrication of graphene nanoribbons. *Nature*, 466(7305):

470–473, 2010.

² Yen-Chia Chen, Dimas G. de Oteyza, Zahra Pedramrazi, Chen Chen, Felix R. Fischer, and Michael F. Crommie. Tuning the band gap of graphene nanoribbons synthesized from molecular precursors. *ACS Nano*, 7(7):6123–6128, 2013.

- ³ Richard Denk, Michael Hohage, Peter Zeppenfeld, Jiming Cai, Carlo A. Pignedoli, Hajo Söde, Roman Fasel, Xinliang Feng, Klaus Müllen, Shudong Wang, Deborah Prezzi, Andrea Ferretti, Alice Ruini, Elisa Molinari, and Pascal Ruffieux. Exciton-dominated optical response of ultra-narrow graphene nanoribbons. *Nat. Commun.*, 5: 4253, 2014.
- ⁴ Jiming Cai, Carlo A. Pignedoli, Leopold Talirz, Pascal Ruffieux, Hajo Söde, Liangbo Liang, Vincent Meunier, Reinhard Berger, Rongjin Li, Xinliang Feng, Klaus Müllen, and Roman Fasel. Graphene nanoribbon heterojunctions. *Nature Nanotech.*, 9:896–900, 2014.
- ⁵ Yen-Chia Chen, Ting Cao, Chen Chen, Zahra Pedramrazi, Danny Haberer, Dimas G. de Oteyza, Felix R. Fischer, Steven G. Louie, and Michael F. Crommie. Molecular bandgap engineering of bottom-up synthesized graphene nanoribbon heterojunctions. *Nature Nanotech.*, 10:156–160, 2015.
- ⁶ Shigeki Kawai, Shohei Saito, Shinichiro Osumi, Shigehiro Yamaguchi, Adam S. Foster, Peter Spijker, and Ernst Meyer. Atomically controlled substitutional boron-doping of graphene nanoribbons. *Nat. Commun.*, 6:8098, 2015.
- ⁷ Ryan R. Cloke, Tomas Marangoni, Giang D. Nguyen, Trinity Joshi, Daniel J. Rizzo, Christopher Bronner, Ting Cao, Steven G. Louie, Michael F. Crommie, and Felix R. Fischer. Site-specific substitutional boron doping of semiconducting armchair graphene nanoribbons. *J. Am. Chem. Soc.*, 137(28):8872–8875, 2015.
- ⁸ Timothy H. Vo, U. Gayani E. Perera, Mikhail Shekhirev, Mohammad Mehdi Pour, Donna A. Kunkel, Haidong Lu, Alexei Gruverman, Eli Sutter, Mircea Cotlet, Dmytro Nykypanchuk, Percy Zahl, Axel Enders, Alexander Sinit-skii, and Peter Sutter. Nitrogen-doping induced self-assembly of graphene nanoribbon-based two-dimensional and three-dimensional metamaterials. *Nano Lett.*, 15(9): 5770–5777, 2015.
- ⁹ Haiming Zhang, Haiping Lin, Kewei Sun, Long Chen, Yulian Zagranyski, Nabi Aghdassi, Steffen Duhm, Qing Li, Dingyong Zhong, Youyong Li, Klaus Müllen, Harald Fuchs, and Lifeng Chi. On-surface synthesis of rylene-type graphene nanoribbons. *J. Am. Chem. Soc.*, 137(12):4022–4025, 2015.
- ¹⁰ Amina Kimouche, Mikko M. Ervasti, Robert Drost, Simo Halonen, Ari Harju, Pekka M. Joensuu, Jani Sainio, and Peter Liljeroth. Ultra-narrow metallic armchair graphene nanoribbons. *Nat. Commun.*, 6:10177, 2015.
- ¹¹ Pascal Ruffieux, Shiyong Wang, Bo Yang and Carlos Sánchez-Sánchez, Jia Liu, Thomas Dienel, Leopold Talirz, Prashant Shinde, Carlo A. Pignedoli, Daniele Passerone, Tim Dumslaff, Xinliang Feng, Klaus Müllen, and Roman Fasel. On-surface synthesis of graphene nanoribbons with zigzag edge topology. *Nature*, 531(7151):489–492, 2016.
- ¹² Dimas G. de Oteyza, Aran García-Lekue, Manuel Vilas-Varela, Néstor Merino-Díez, Eduard Carbonell-Sanromà, Martina Corso, Guillaume Vasseur, Celia Rogero, Enrique Guitin, Jose Ignacio Pascual, J. Enrique Ortega, Yutaka Wakayama, and Diego Peña. Substrate-independent growth of atomically precise chiral graphene nanoribbons. *ACS Nano*, 10(9):9000–9008, 2016.
- ¹³ Leopold Talirz, Pascal Ruffieux, and Roman Fasel. On-surface synthesis of atomically precise graphene nanoribbons. *Adv. Mater.*, 28(29):6222–6231, 2016.
- ¹⁴ Ivan A. Verzhbitskiy, Marzio De Corato, Alice Ruini, Elisa Molinari, Akimitsu Narita, Yunbin Hu, Matthias G. Schwab, Matteo Bruna, Duhee Yoon, Silvia Milana, Xinliang Feng, Klaus Müllen, Andrea C. Ferrari, Cinzia Casiraghi, and Deborah Prezzi. Raman fingerprints of atomically precise graphene nanoribbons. *Nano Lett.*, 16(6): 3442–3447, 2016.
- ¹⁵ Shiyong Wang, Leopold Talirz, Carlo A. Pignedoli, Xinliang Feng, Klaus Müllen, Roman Fasel, and Pascal Ruffieux. Giant edge state splitting at atomically precise graphene zigzag edges. *Nat. Commun.*, 7:11507, 2016.
- ¹⁶ B. V. Senkovskiy, M. Pfeiffer, S. K. Alavi, A. Bliesener, J. Zhu, S. Michel, A. V. Fedorov, R. German, D. Hertel, D. Haberer, L. Petaccia, F. R. Fischer, K. Meerholz, P. H. M. van Loosdrecht, K. Lindfors, and A. Grüneis. Making graphene nanoribbons photoluminescent. *Nano Lett.*, 17(7):4029–4037, 2017.
- ¹⁷ Hironobu Hayashi, Junichi Yamaguchi, Hideyuki Jippo, Ryunosuke Hayashi, Naoki Aratani, Mari Ohfuchi, Shintaro Sato, and Hiroko Yamada. Experimental and theoretical investigations of surface-assisted graphene nanoribbon synthesis featuring carbon-fluorine bond cleavage. *ACS Nano*, 11(6):6204–6210, 2017.
- ¹⁸ Meizhuang Liu, Mengxi Liu, Limin She, Zeqi Zha, Jinliang Pan, Shichao Li, Tao Li, Yangyong He, Zeying Cai, Jiaobing Wang, Yue Zheng, Xiaohui Qiu, and Dingyong Zhong. Graphene-like nanoribbons periodically embedded with four- and eight-membered rings. *Nat. Commun.*, 8: 14924, 2017.
- ¹⁹ Shiyong Wang, Neerav Kharche, Eduardo Costa Girão, Xinliang Feng, Klaus Müllen, Vincent Meunier, Roman Fasel, and Pascal Ruffieux. Quantum dots in graphene nanoribbons. *Nano Lett.*, 17(7):4277–4283, 2017.
- ²⁰ Eduard Carbonell-Sanromà, Jeremy Hieulle, Manuel Vilas-Varela, Pedro Brandimarte, Mikel Iraola, Ana Barragán, Jingcheng Li, Mikel Abadia, Martina Corso, Daniel Sánchez-Portal, Diego Peña, and Jose Ignacio Pascual. Doping of graphene nanoribbons via functional group edge modification. *ACS Nano*, 11(7):7355–7361, 2017.
- ²¹ Giang D. Nguyen, Hsin-Zon Tsai, Tomas Marangoni Arash A. Omrani, Meng Wu, Daniel J. Rizzo, Griffin F. Rodgers, Ryan R. Cloke, Rebecca A. Durr, Yuki Sakai, Franklin Liou, Andrew S. Aikawa, James R. Chelikowsky, Steven G. Louie, Felix R. Fischer, and Michael F. Crommie. Atomically precise graphene nanoribbon heterojunctions from a single molecular precursor. *Nature Nanotech.*, 2017.
- ²² Matthias Koch, Francisco Ample, Christian Joachim, and Leonhard Grill. Voltage-dependent conductance of a single graphene nanoribbon. *Nature Nanotech.*, 7:713717, 2012.
- ²³ Patrick B. Bennett, Zahra Pedramrazi, Ali Madani, Yen-Chia Chen, Dimas G. de Oteyza, Chen Chen, Felix R. Fischer, Michael F. Crommie, and Jeffrey Bokor. Bottom-up graphene nanoribbon field-effect transistors. *Appl. Phys. Lett.*, 103(25):253114, 2013.
- ²⁴ Okan Deniz, Carlos Sánchez-Sánchez, Tim Dumslaff, Xinliang Feng, Akimitsu Narita, Klaus Müllen, Neerav Kharche, Vincent Meunier, Roman Fasel, and Pascal Ruffieux. Revealing the electronic structure of silicon intercalated armchair graphene nanoribbons by scanning tunneling spectroscopy. *Nano Lett.*, 17(4):2197–2203, 2017.
- ²⁵ Boris V. Senkovskiy, Alexander V. Fedorov, Danny Haberer, Mani Farjam, Konstantin A. Simonov, Alexei B. Preobrajenski, Niels Mårtensson, Nicolae Atodiresi, Vasile Caciuc, Stefan Blügel, Achim Rosch, Nikolay I. Verbitskiy, Martin Hell, Daniil V. Evtushinsky, Raphael German, Tomas Marangoni, Paul H. M. van Loosdrecht, Fe-

- lix R. Fischer, and Alexander Grüneis. Semiconductor-to-metal transition and quasiparticle renormalization in doped graphene nanoribbons. *Adv. Electron. Mater.*, 3(4):1600490, 2017.
- ²⁶ Chuanxu Ma, Liangbo Liang, Zhongcan Xiao, Alexander A. Puzetky, Kunlun Hong, Wenchang Lu, Vincent Meunier, J. Bernholc, and An-Ping Li. Seamless staircase electrical contact to semiconducting graphene nanoribbons. *Nano Lett.*, 17(10):6241–6247, 2017.
- ²⁷ Eduard Carbonell-Sanromà, Pedro Brandimarte, Richard Balog, Martina Corso, Shigeki Kawai, Aran Garcia-Lekue, Shohei Saito, Shigehiro Yamaguchi, Ernst Meyer, Daniel Sanchez-Portal, and Jose Ignacio Pascual. Quantum dots embedded in graphene nanoribbons by chemical substitution. *Nano Letters*, 17(1):50–56, 2017.
- ²⁸ S. Linden, D. Zhong, A. Timmer, N. Aghdassi, J. H. Franke, H. Zhang, X. Feng, K. Müllen, H. Fuchs, L. Chi, and H. Zacharias. Electronic structure of spatially aligned graphene nanoribbons on au(788). *Phys. Rev. Lett.*, 108:216801, 2012.
- ²⁹ Pascal Ruffieux, Jinming Cai, Nicholas C. Plumb, Luc Patthey, Deborah Prezzi, Andrea Ferretti, Elisa Molinari, Xinliang Feng, Klaus Müllen, Carlo A. Pignedoli, and Roman Fasel. Electronic structure of atomically precise graphene nanoribbons. *ACS Nano*, 6(8):6930–6935, 2012.
- ³⁰ Konstantin A. Simonov, Nikolay A. Vinogradov, Alexander S. Vinogradov, Alexander V. Generalov, Gleb I. Svirskiy, Attilio A. Cafolla, Nils Mårtensson, and Alexei B. Preobrazjenski. Effect of electron injection in copper-contacted graphene nanoribbons. *Nano Res.*, 9(9):2735–2746, 2016.
- ³¹ Boris V. Senkovskiy, Danny Haberer, Dmitriy Yu. Usachov, Alexander V. Fedorov, Niels Ehlen, Martin Hell, Rebecca Durr A., Felix R. Fischer, and Alexander Grüneis. Spectroscopic characterization of n=9 armchair graphene nanoribbons. *Phys. Status Solidi RRL*, 11(8):1700157, 2017.
- ³² Hajo Söde, Leopold Talirz, Oliver Gröning, Carlo Antonio Pignedoli, Reinhard Berger, Xinliang Feng, Klaus Müllen, Roman Fasel, and Pascal Ruffieux. Electronic band dispersion of graphene nanoribbons via fourier-transformed scanning tunneling spectroscopy. *Phys. Rev. B*, 91:045429, 2015.
- ³³ Leopold Talirz, Hajo Sde, Tim Dumslaff, Shiyong Wang, Juan Ramon Sanchez-Valencia, Jia Liu, Prashant Shinde, Carlo A. Pignedoli, Liangbo Liang, Vincent Meunier, Nicholas C. Plumb, Ming Shi, Xinliang Feng, Akimitsu Narita, Klaus Müllen, Roman Fasel, and Pascal Ruffieux. On-surface synthesis and characterization of 9-atom wide armchair graphene nanoribbons. *ACS Nano*, 11(2):1380–1388, 2017.
- ³⁴ Guillaume Vasseur, Yannick Fagot-Revurat, Muriel Sicot, Bertrand Kierren, Luc Moreau, Daniel Malterre, Luis Cardenas, Gianluca Galeotti, Josh Lipton-Duffin, Federico Rosei, Marco Di Giovannantonio, Giorgio Contini, Patrick Le Fvre, Francois Bertran, Liangbo Liang, Vincent Meunier, and Dmitrii F. Perepichka. Quasi one-dimensional band dispersion and surface metallization in long-range ordered polymeric wires. *Nat. Commun.*, 7:10235, 2016.
- ³⁵ Andrea Basagni, Guillaume Vasseur, Carlo A. Pignedoli, Manuel Vilas-Varela, Diego Pea, Louis Nicolas, Lucia Vitali, Jorge Lobo-Checa, Dimas G. de Oteyza, Francesco Sedona, Maurizio Casarin, J. Enrique Ortega, and Mauro Sambi. Tunable band alignment with unperturbed carrier mobility of on-surface synthesized organic semiconducting wires. *ACS Nano*, 10(2):2644–2651, 2016.
- ³⁶ Guillaume Vasseur, Mikel Abadia, Luis A. Miccio, Jens Brede, Aran Garcia-Lekue, Dimas G. de Oteyza, Celia Rogero, Jorge Lobo-Checa, and J. Enrique Ortega. II band dispersion along conjugated organic nanowires synthesized on a metal oxide semiconductor. *J. Am. Chem. Soc.*, 138(17):5685–5692, 2016.
- ³⁷ Huaixiu Zheng, Z. F. Wang, Tao Luo, Q. W. Shi, and Jie Chen. Analytical study of electronic structure in armchair graphene nanoribbons. *Phys. Rev. B*, 75:165414, 2007.
- ³⁸ Katsunori Wakabayashi, Ken ichi Sasaki, Takeshi Nakanishi, and Toshiaki Enoki. Electronic states of graphene nanoribbons and analytical solutions. *Sci. Technol. Adv. Mater.*, 11(5):054504, 2010.
- ³⁹ Ken” ichi Sasaki, Katsunori Wakabayashi, and Toshiaki Enoki. Electron wave function in armchair graphene nanoribbons. *J. Phys. Soc. Jpn.*, 80(4):044710, 2011.
- ⁴⁰ G. Koller, S. Berkebile, M. Oehzelt, P. Puschnig, C. Ambrosch-Draxl, F. P. Netzer, and M. G. Ramsey. Intra- and intermolecular band dispersion in an organic crystal. *Science*, 317:351–355, 2007.
- ⁴¹ Peter Puschnig, Stephen Berkebile, Alexander J. Fleming, Georg Koller, Konstantin Emtsev, Thomas Seyller, John D. Riley, Claudia Ambrosch-Draxl, Falko P. Netzer, and Michael G. Ramsey. Reconstruction of molecular orbital densities from photoemission data. *Science*, 326:702–706, 2009.
- ⁴² Peter Puschnig and Daniel Lüftner. Simulation of angle-resolved photoemission spectra by approximating the final state by a plane wave: From graphene to polycyclic aromatic hydrocarbon molecules. *J. Electron Spectrosc. Relat. Phenom.*, 200(Supplement C):193 – 208, 2015. Special Anniversary Issue: Volume 200.
- ⁴³ A. Mugarza, A. Mascaraque, V. Repain, S. Rousset, K. N. Altmann, F. J. Himpsel, Yu. M. Koroteev, E. V. Chulkov, F. J. García de Abajo, and J. E. Ortega. Lateral quantum wells at vicinal au(111) studied with angle-resolved photoemission. *Phys. Rev. B*, 66:245419, 2002.
- ⁴⁴ A. Mugarza, J. E. Ortega, F. J. Himpsel, and F. J. García de Abajo. Measurement of electron wave functions and confining potentials via photoemission. *Phys. Rev. B*, 67:081404, 2003.
- ⁴⁵ Eric L. Shirley, L. J. Terminello, A. Santoni, and F. J. Himpsel. Brillouin-zone-selection effects in graphite photoelectron angular distributions. *Phys. Rev. B*, 51:13614–13622, 1995.
- ⁴⁶ Aaron Bostwick, Taisuke Ohta, Thomas Seyller, Karsten Horn, and Eli Rotenberg. Quasiparticle dynamics in graphene. *Nat. Phys.*, 3:36–40, 2007.
- ⁴⁷ M. Mucha-Kruczyński, O. Tsypliyatyev, A. Grishin, E. McCann, Vladimir I. Fal’ko, Aaron Bostwick, and Eli Rotenberg. Characterization of graphene through anisotropy of constant-energy maps in angle-resolved photoemission. *Phys. Rev. B*, 77:195403, 2008.
- ⁴⁸ Isabella Gierz, Jürgen Henk, Hartmut Höchst, Christian R. Ast, and Klaus Kern. Illuminating the dark corridor in graphene: Polarization dependence of angle-resolved photoemission spectroscopy on graphene. *Phys. Rev. B*, 83:121408, 2011.
- ⁴⁹ Y. Liu, G. Bian, T. Miller, and T.-C. Chiang. Visualizing electronic chirality and berry phases in graphene systems using photoemission with circularly polarized light. *Phys. Rev. Lett.*, 107:166803, 2011.

- ⁵⁰ Choongyu Hwang, Cheol-Hwan Park, David A. Siegel, Alexei V. Fedorov, Steven G. Louie, and Alessandra Lanzara. Direct measurement of quantum phases in graphene via photoemission spectroscopy. Phys. Rev. B, 84:125422, 2011.
- ⁵¹ Sung Won Jung, Woo Jong Shin, Jimin Kim, Luca Moreschini, Han Woong Yeom, Eli Rotenberg, Aaron Bostwick, and Keun Su Kim. Sublattice interference as the origin of σ band kinks in graphene. Phys. Rev. Lett., 116:186802, 2016.
- ⁵² Taisuke Ohta, Aaron Bostwick, J. L. McChesney, Thomas Seyller, Karsten Horn, and Eli Rotenberg. Interlayer interaction and electronic screening in multilayer graphene investigated with angle-resolved photoemission spectroscopy. Phys. Rev. Lett., 98:206802, 2007.
- ⁵³ P. M. Sheverdyaeva, R. Requist, P. Moras, S. K. Mathatha, M. Papagno, L. Ferrari, E. Tosatti, and C. Carbone. Energy-momentum mapping of d -derived au(111) states in a thin film. Phys. Rev. B, 93:035113, 2016.
- ⁵⁴ D. C. Elias, R. V. Gorbachev, A. S. Mayorov, S. V. Morozov, A. A. Zhukov, P. Blake, L. A. Ponomarenko, I. V. Grigorieva, K. S. Novoselov, F. Guinea, and A. K. Geim. Dirac cones reshaped by interaction effects in suspended graphene. Nat. Phys., 7:701704, 2011.
- ⁵⁵ Julia Tesch, Philipp Leicht, Felix Blumenschein, Luca Gagnaniello, Mikhail Fonin, Lukas Eugen Marsoner Steinkasserer, Beate Paulus, Elena Voloshina, and Yuriy Dedkov. Structural and electronic properties of graphene nanoflakes on au(111) and ag(111). Sci. Rep., 6:23439, 2016.
- ⁵⁶ Klaus Koepf and Helmut Eschrig. Full-potential nonorthogonal local-orbital minimum-basis band-structure scheme. Phys. Rev. B, 59:1743–1757, 1999. FPLO, <http://www.FPLO.de/>.